Research article

Interleukin-10 induces TNF-driven apoptosis and ROS production in salivary gland cancer cells

Maksym Skrypnyk [a], Tetiana Yatsenko [a], Oleksandra Riabets [a], Yousef Salama [b], Margarita Skikevych [c], Taro Osada [d], Morikuni Tobita [e], Satoshi Takahashi [f], Koichi Hattori [g,1,**], Beate Heissig [a,1,*]

[a] *Department of Research Support Utilizing Bioresource Bank, Graduate School of Medicine, Juntendo University School of Medicine, 2-1-1 Hongo, Bunkyo-Ku, Tokyo 113-8421, Japan*
[b] *An-Najah Center for Cancer and Stem Cell Research, Faculty of Medicine and Health Sciences, An-Najah National University, P.O. Box 7, Nablus 99900800, Palestine*
[c] *Department of Surgical Dentistry and Maxillofacial Surgery with Plastic and Reconstructive Surgery of Head and Neck, Poltava State Medical University, 23 Shevchenko Street. Poltava, Ukraine*
[d] *Department of Gastroenterology Juntendo University Urayasu Hospital, Japan*
[e] *Department of Oral and Maxillofacial Surgery, Juntendo University School of Medicine, Japan*
[f] *Division of Clinical Precision Research Platform, The Institute of Medical Science, The University of Tokyo, 4-6-1 Shirokanedai, Minato-ku, Tokyo 108-8639, Japan*
[g] *Center for Genome and Regenerative Medicine, Juntendo University, Graduate School of Medicine, 2-1-1 Hongo, Bunkyo-Ku, Tokyo 113-8421, Japan*

A B S T R A C T

Treatment resistance after chemo-/immunotherapy occurs in patients with head and neck squamous cell cancers (HNSCs), including salivary gland cancers (SGCs). Interleukin-10 (IL-10), a cytokine with pro- and anti-cancer effects, has an unclear impact on HNSC/SGC cells. We show that HNSC patients exhibiting high expression of IL-10 and its receptor IL-10Rα experience have prolonged overall survival. Immunoreactive IL-10 was low in ductal cells of human SGC biopsies. Human (A253) and murine WR21-SGC cells expressed IL-10Rβ, but only A253 cells expressed IL-10 and IL-10Rα. The addition of recombinant IL-10 impaired SGC cell proliferation and induced apoptosis *in vitro*. N-acetylcysteine restored IL-10-induced reactive oxygen species (ROS) production but did not prevent IL-10-mediated viability loss. Mechanistically, recIL-10 delayed cell cycle progression from G0/G1 to the S phase with *cyclin D* downregulation and upregulation of NF-kB. IL-10 increased tumor necrosis factor-α (TNF-α) in A253 and WR21 and *FasL* in WR21 cells. Neutralizing antibodies against TNF-α and NF-kB inhibition restored SGC proliferation after IL-10 treatment, emphasizing the critical role of TNF-α and NF-kB in IL-10-mediated anti-tumor effects. These findings underscore the potential of IL-10 to impede SGC cell growth through

---

* Corresponding author. Dep. of Research Support Utilizing Bioresource Bank Juntendo University, Graduate School of Medicine 2-1-1 Hongo, Bunkyo-ku Tokyo, 113-8421, Japan.
** Corresponding author.
E-mail addresses: maksym.skrypnyk@students.mq.edu.au (M. Skrypnyk), tetyanaa.yatsenko@gmail.com (T. Yatsenko), o.riabets.lb@juntendo.ac.jp (O. Riabets), yousef.ut@najah.edu (Y. Salama), skikevich1959@gmail.com (M. Skikevych), otaro@juntendo.ac.jp (T. Osada), mtobita@juntendo.ac.jp (M. Tobita), radius@ims.u-tokyo.ac.jp (S. Takahashi), khattori@juntendo.ac.jp (K. Hattori), heissig@juntendo.ac.jp (B. Heissig).
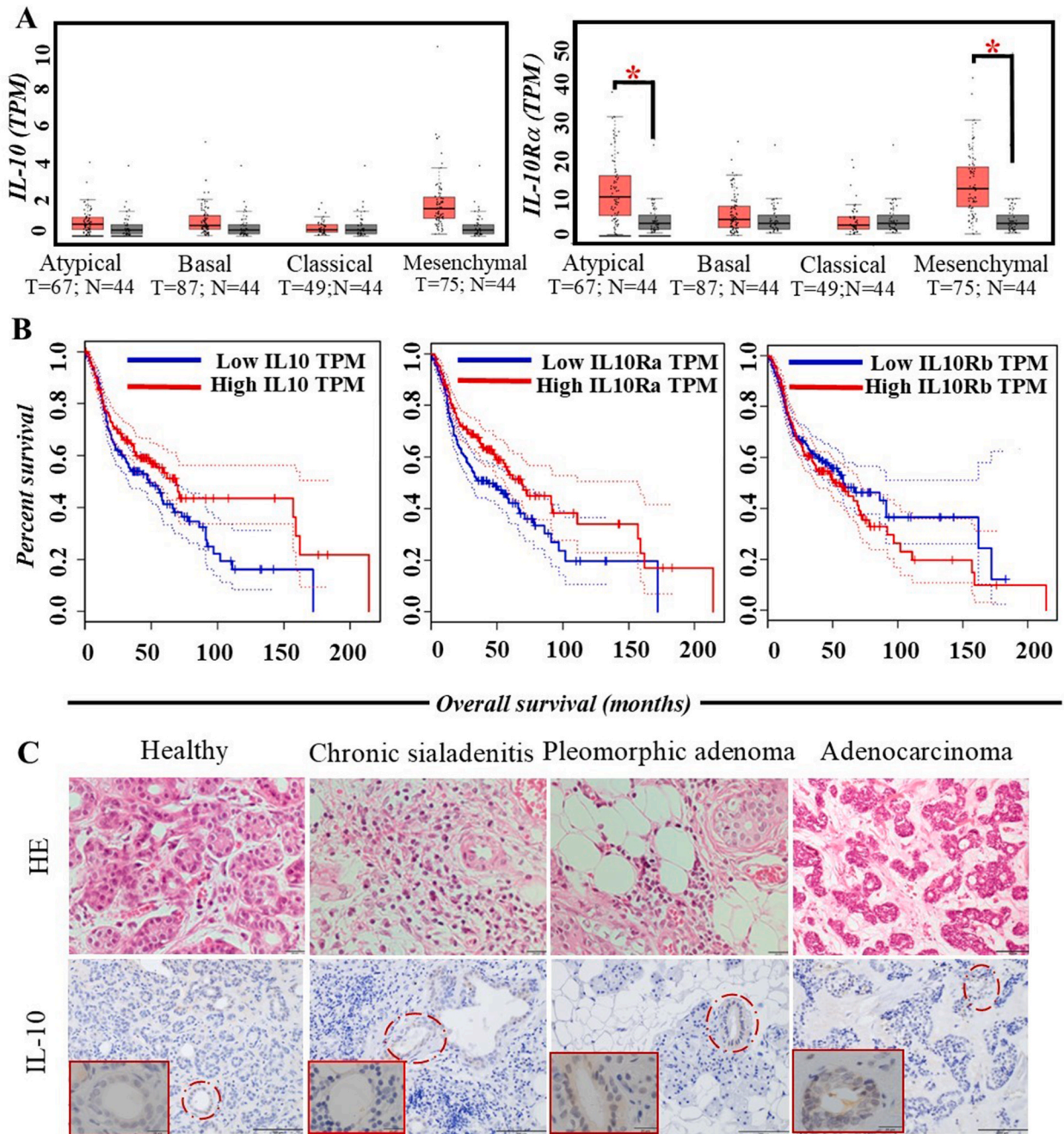[1] These authors share senior authorship.

Fig. 1. IL-10 and IL-10 receptor α expression correlate with better survival outcomes in head and neck squamous cell carcinoma patients.
A. Expression of Interleukin-10 (IL-10) and IL-10 receptor α (IL-10Rα) in cancer and adjacent normal tissues of indicated histological subtypes of Head and Neck squamous cell carcinoma (HNSC) as determined in-silico using GEPIA. The red boxes represent cancer samples, and the gray boxes represent non-malignant samples. B. Kaplan-Meier plots showing overall survival of HNSC patients with high (red line) and low (blue) *IL*-10 mRNA expression (left panel) (IL-10 Logrank p = 0.039, HR(high) = 0.75, p(HR) = 0.04, n(high) = 256, n(low) = 259), IL-10Rα mRNA (middle panel), (IL-10Rα Logrank p = 0.043, HR(high) = 0.68, p(HR) = 0.0046, n(high) = 258, n(low) = 259), IL-10Rβ mRNA (right panel) (IL-10Rβ Logrank p = 0.046, HR(high) = 1.1, p(HR) = 0.46, n(high) = 259, n(low) = 259). Patient stratification according to their IL-10, IL-10Rα, and IL-10Rβ levels was determined using GEPIA datasets http://gepia.cancer-pku.cn/. TPM, transcripts per million. C. Representative images of Hematoxylin&Eosin (H&E; upper panel)- and IL-10-immuno-stained (lower panel; brown staining) sections of non-diseased, inflamed (chronic sialadenitis), premalignant (pleomorphic adenoma), and solid cancer (adenocarcinoma) tissue sections. Scale bar = 200 μm. (For interpretation of the references to colour in this figure legend, the reader is referred to the Web version of this article.)

apoptosis induction, unraveling potential therapeutic targets for intervention in salivary gland carcinomas.

1. Introduction

Head and neck squamous cell cancers (HNSCs) pose significant challenges in treatment due to their rarity and inherent resistance [1]. They comprise ~4 % of all cancers in the United States (www.cancer.net/cancer-types/head-and-neck-cancer/statistics), and salivary gland (SG) cancers (SGCs) account for ~5 % of HNSCs. The 5-year relative survival rate of HNSCs, including SGCs, ranges between ~60 and 90 %, contingent upon histological cell type and metastasis status. Predominantly of epithelial origin, SG neoplasms, with 70 % being pleomorphic adenomas, also include histological types such as mucoepidermoid carcinoma [2]. The primary treatment for SGC involves surgery [3], while alternative therapy like chemotherapy, radiotherapy, and targeted immunotherapy have shown limited efficacy, necessitating the search for novel treatment avenues [4,5].

The SG constantly interacts with external pathogens, so the local immune system is continuously challenged and seems to influence the development of HNSCs. Interleukin-10 (IL-10), an anti-inflammatory cytokine, signals through a receptor complex of IL-10Rα and IL-10Rβ [6]. While IL-10Rβ interacts with IL-10, IL-22/-26/-28 and IL-29 [7], IL-10Rα exclusively binds IL-10.

IL-10-deficient mice develop tumors at a higher rate [8]. Depending on the tumor type, IL-10 may exert pro- or anti-tumor effects [8–10]. IL-10 is expressed in normal, benign, and malignant SG tumors with different intensities [11,12] and is detected in saliva [11, 13]. However, the impact of exogenous IL-10 on SGC growth is poorly understood.

Evasion from apoptosis, a hallmark of cancer, is manifested in SG adenoid cystic carcinoma, where apoptosis-associated proteins are prognosticators for poor survival [14]. Under physiological conditions, tumor necrosis factor-α (TNF-α) induces the pro-apoptotic pathway triggered by procaspase 8 cleavage and is induced after Nuclear Factor kB (NF-kB) activation. TNFR1 activation by TNF-α reduces mitochondrial membrane potentials, triggering the production of mitochondrial reactive oxidative species (ROS) [15]. TNF-α-mediated NF-kB activation through catalase and SOD causes TNF-α expression that feedback into ROS generation (reviewed in Ref. [16]. TNFR1 and TNFR2 signaling can lead to NF-kB activation. TNFR2 engagement promotes cell survival via this pathway [17]. Previous research demonstrated that autoantibodies of patients with Sjoegren disease caused apoptosis of primary human SG epithelial cells via an extrinsic apoptotic pathway through the production of TNF-α, treatment with blockers of TNF-α with adalimumab and etanercept prevented SG epithelial cells apoptosis [18]. Furthermore, TNF-α inhibitors were found to block the apoptosis of human epithelial cells in salivary glands, suggesting an apoptosis-enhancing role for TNF-α in SGC cells.

IL-10 can block NF-kB activity [19]. NF-kB controls the expression of TNF-α and death factors like Fas or bax [20], thereby influencing immune homeostasis and cancer cell survival. The NF-kB inhibitor JSH-23 inhibits NF-kB transcriptional activity without affecting IκB degradation and attenuates apoptosis in osteoblasts by reducing ROS production and enhancing Nrf2/HO-1 expression [21].

Motivated by promising reports on the anti-tumor effects of IL-10 in solid cancers, we investigated whether IL-10 is produced in SGC cells and its role in SGC apoptosis. Our findings reveal that the human A253 and murine WR21 SGC cells express low IL-10 and high IL-10Rβ subunit levels. Still, only A253 cancer cells co-express IL-10Rα. IL-10 addition suppressed SGC cell proliferation and induced apoptosis through upregulation of TNF-α, accompanied by ROS production and enhanced NF-kB expression in SGC cells. This study sheds light on the potential therapeutic implications of IL-10 in SGCs, paving the way for further preclinical investigations and clinical considerations.

2. Results

2.1. Expression of IL-10 and its receptors in human SG cancer (SGC) tissues and cell lines

Using the web-based bioinformatic tool GEPIA, we tested IL-10, IL-10 receptor α (IL-10Rα), or IL-10Rβ transcript expression in

Table 1
Overview of the clinical submandibular SG specimens under investigation with detailed information on histopathological classification, age, and gender.

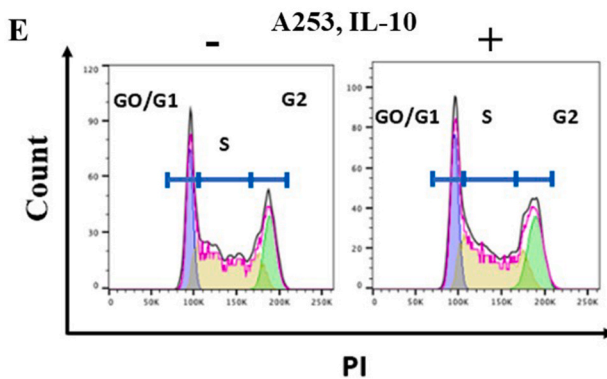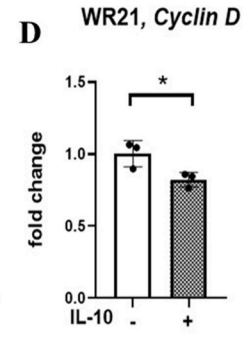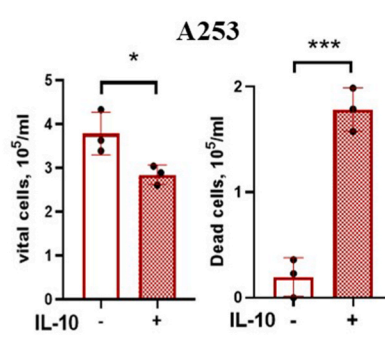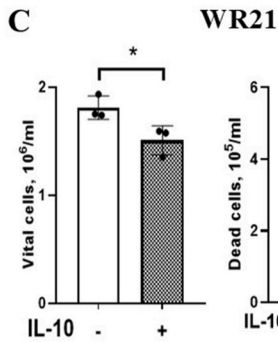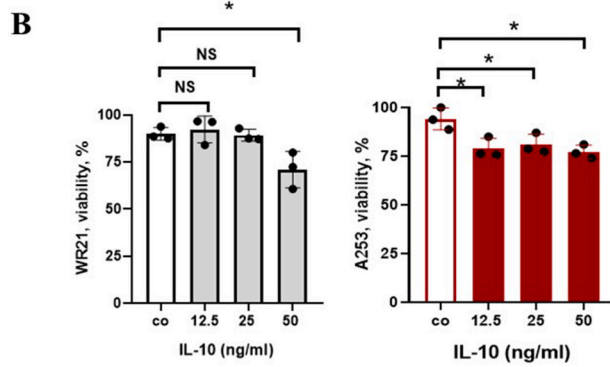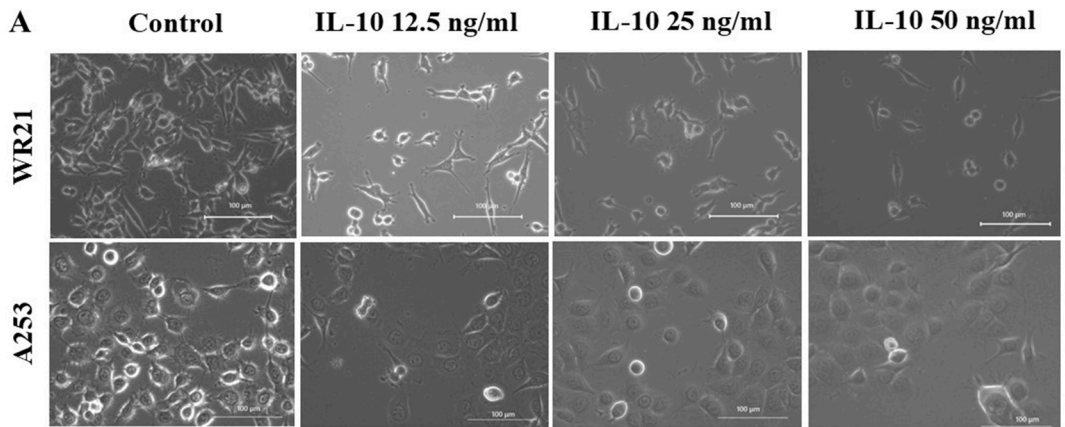| №	Age, gender	Diagnosis	Race
1	48, male	Calculous sialadenitis of submandibular salivary gland (pathology biopsy including adjacent tissues)	Caucasian
2	60, female	Chronic sialadenitis of submandibular salivary gland	Caucasian
3	51, male	Pleomorphic adenoma of submandibular salivary gland	Caucasian
4	45, female	Adenocystic carcinoma of parotid salivary gland	Caucasian
5	31, male	Calculous sialadenitis of submandibular salivary gland (pathology biopsy including adjacent tissues)	Caucasian
6	34, female	Pleomorphic adenoma of parotid salivary gland	Caucasian
7	50, female	Pleomorphic adenoma of parotid salivary gland	Caucasian
8	20, male	Pleomorphic adenoma of parotid salivary gland	Caucasian
9	42, male	Exacerbation of chronic submandibular sialadenitis	Caucasian
10	43, female	Calculous sialadenitis of submandibular salivary gland	Caucasian
11	52, female	Calculous sialadenitis of the submandibular salivary gland	Caucasian
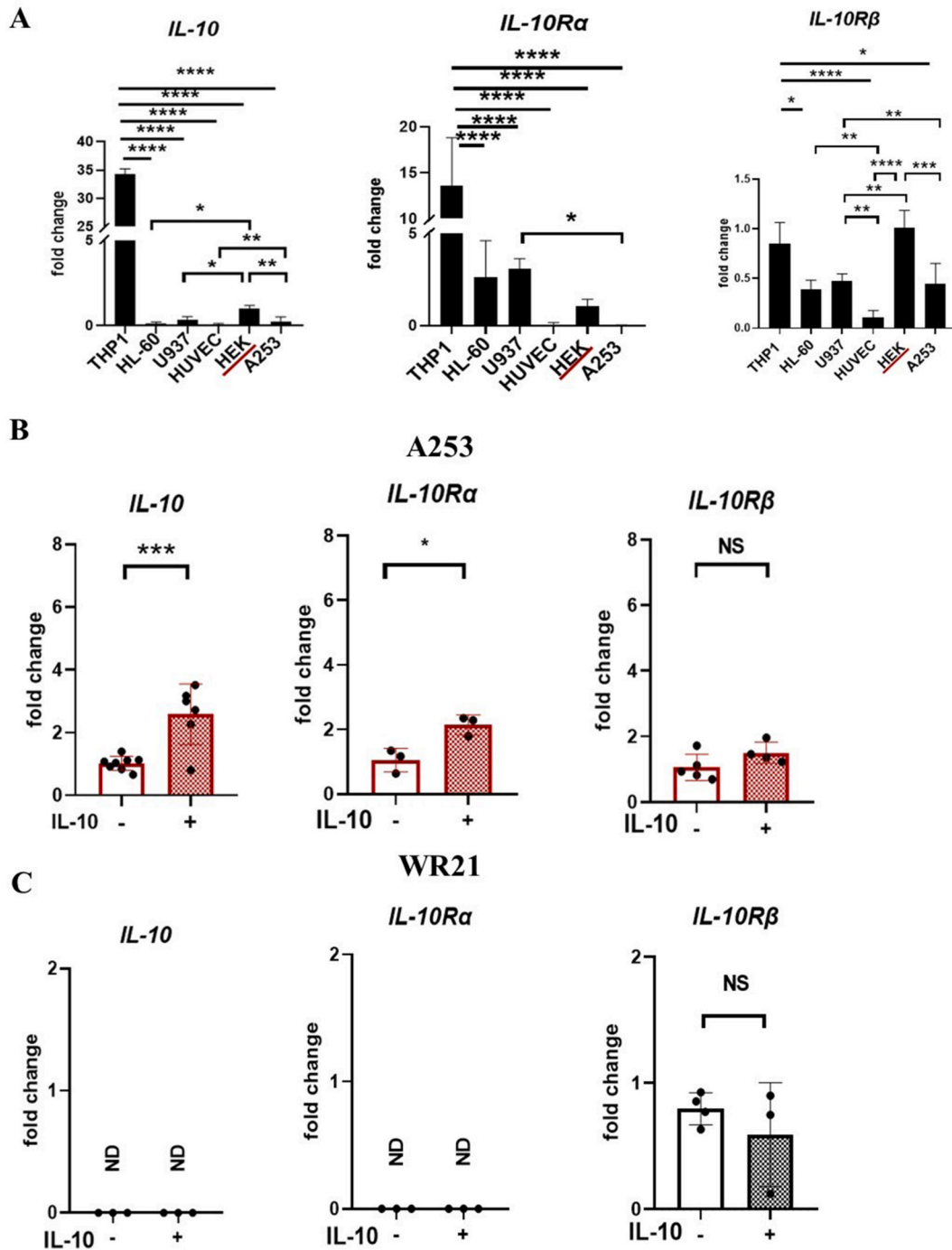
Fig. 2. The human A253 and mouse WR21 SGC cells express IL-10β, but only A253 cells show low IL-10 or IL-10*Ra* expression **A.** Fold changes of *IL-10, IL-10Ra,* and *IL-10Rβ* expression in human cell lines as determined by qPCR. The following cell types were included: myeloid hematopoietic (THP-1, U937, HL-60), immortalized endothelial (HUVEC) and embryonic kidney (HEK), or salivary gland epidermoid carcinoma cells (A253) (n = 3/group). Expression of the target gene was normalized to *β-actin* expression in the same samples. Fold change in gene expression was normalized to the expression of the red underlined cell line (HEK) indicated in each panel. **B–C.** Fold changes in *IL-10, IL-10Ra,* and *IL-10Rβ* expression as determined by qPCR in human and epidermoid carcinoma A253 (B) and murine adenocarcinoma WR21 (C) cells treated with/without recIL-10. Expression of the target gene was normalized to *β-actin* expression in the same samples. Fold change in gene expression was normalized to the expression in the control samples.*p < 0.05, **p < 0.01, ***p < 0.001, ****p < 0.0001 using two-way ANOVA or Student's t-test with mean and SD depicted. (For interpretation of the references to colour in this figure legend, the reader is referred to the Web version of this article.)

A

| | Control | IL-10 12.5 ng/ml | IL-10 25 ng/ml | IL-10 50 ng/ml |

B

WR21, viability, % vs IL-10 (ng/ml): co, 12.5, 25, 50

A253, viability, % vs IL-10 (ng/ml): co, 12.5, 25, 50

C WR21 | A253

D WR21, *Cyclin D*

E A253, IL-10

Cell cycle		A253	WR21
Co	G0/G1	23.5±1.3	51.8±0.3
	S	53±1.5	36±0.7
	G2	22.5±3.2	11.5±0.5
IL-10	G0/G1	27.6±0.6**	53±0.9
	S	49±0.1*	35.4±0.5
	G2	23±1.7	11.2±0.5

(caption on next page)

Fig. 3. Treatment with recIL-10 impairs SGC viability and causes cell cycle arrest A. Representative light macroscopic images of the murine WR21 and human A253 SGC cells were treated with different concentrations of recIL-10 for 24 h. Scale bar = 100 μm. B. The viability rate of indicated cells treated with/without shown doses of recIL-10 was determined by trypan blue exclusion (n = 3/group). C. The absolute number of dead and viable IL-10-treated and control WR21 and A253 cells after 24 h in culture was determined using the Trypan blue exclusion assay (n = 3/group). D. Fold change in *Cyclin D* expression of control or IL-10-treated WR21 cells as determined by qPCR. Data were analyzed using the relative quantification method with normalization to *β-actin* and relative to controls. Each sample was analyzed at least in triplicate, and the average fold change was determined. Each dot represents the result of one cell sample. E. A representative histogram showing the cell-cycle analysis of control- and IL-10-treated A253 and WR21 cells after a 24-h culture period as determined by flow cytometry (n = 3/group). Left panel: an example of the histograms obtained from analyzing A253 cells. Right panel: Table summarizing the % of cells in indicated cell cycle phases. *p < 0.05, **p < 0.01, ***p < 0.001, using two-way ANOVA or Student's t-test with mean and SD depicted. (For interpretation of the references to colour in this figure legend, the reader is referred to the Web version of this article.)

different histological subtypes of Head and Neck squamous cell carcinoma (HNSC) compared to normal adjacent tissues. Higher *IL-10Rα*, but not *IL-10β* (data now shown) or *IL-10* expression, was found in atypical and mesenchymal histological subtypes of HNSC compared to normal tissues (Fig. 1A). HNSC patients with higher *IL-10* and *IL-10Rα* expression levels showed better overall survival (p < 0.04, <0.0046, not significant (n.s.), respectively; (Fig. 1B), indicating that the IL-10 signaling pathway has clinical relevance.

The expression of IL10-Rs in HNSCs encouraged us to explore IL-10 signaling further in SGCs, a subgroup of HNSC. We analyzed human SG tissues from healthy subjects, patients with chronic sialadenitis, pleomorphic adenoma, and adenocarcinoma to confirm IL-10 expression in SG cancer tissues of patients with our *in silico* expression data using primary tumor samples of the salivary glands. Patient characteristics are provided in Table 1. Patients with pre-cancerous or SG adenocarcinoma had not received treatment before surgery.

H&E staining results of tissues from randomly selected patients with sialadenitis, where extraction of their SG tissues had been necessary (n = 4), pleomorphic adenoma – a known precancerous SG tumor (n = 4), and adenocarcinoma are shown in Fig. 1C. Peritumoral normal SG tissues served as normal tissues (n = 2).

We used immunohistochemistry to investigate which cell type - cancer cells or cells of the tumor microenvironment, such as inflammatory cells – mainly expressed IL-10 in human SG tissues. IL-10 expression was found in ductal cells of SGs. Ductal cells showed the lowest immunoreactive IL-10 in healthy and inflamed SG tissues, higher levels in pleomorphic adenoma, and the highest immunoreactive IL-10 in adenocarcinoma tissues (Fig. 1C). However, the overall signal was still not strong. No IL-10 signal was detected in infiltrating inflammatory cells in immunostained sections.

Next, we compared *IL-10*, *IL-10Rα*, and *IL-10Rβ* expression in the human A253 SG epidermoid carcinoma cell line of submandibular SG origin with non-SGC cell lines by quantitative PCR (qPCR) (Fig. 2A). The latter included the human cell lines of hematopoietic myeloid (THP1, HL-60, and U937), immortalized endothelial, and embryonic kidney (HUVEC and HEK) origin. The human epidermoid carcinoma A253 cells showed low *IL-10, IL-10Rβ*, and IL-10Rα expression, especially compared to the high expression in hematopoietic myeloid (HL-60 and THP1) and embryonic cells (Fig. 2A). Myeloid cells and HEK cells expressed the highest *IL-10* and *IL-10Rα* transcript levels. These data suggested that SG cancer cells express IL-10Rα and IL-10 at low levels and can respond in a specific way to IL-10 treatment.

2.2. IL-10 amplifies its mRNA in SGC cells

Next, we determined whether IL-10 could affect endogenous IL-10 mRNA synthesis. The human epidermoid carcinoma A253 and mouse adenocarcinoma WR21 SG cells were treated with recIL-10 for 24 h in culture. *IL-10Rβ* was expressed in both cell lines, while *IL-10* and *IL-10Rα* expression were found only in A253 cells. IL-10 exposure enhanced *IL-10* and *IL-10Rα* but not *IL-10Rβ* expression in A253 cells in 24-hr cultures (Fig. 2B). *IL*-10Rs and *IL-10* expression did not change after recIL-10 treatment in murine WR21 cells (Fig. 2C). These results indicate that IL-10 enhanced *IL-10* and *IL-10Rα* transcription in A253 SG cells.

2.3. Impaired SGC growth and cell cycle progression after IL-10 exposure

To examine proliferation in SG cancer cells, we treated mouse WR21 and human A253 cells with recIL-10 ranging from 0 to 50 ng/ml for 24 h. IL-10 treatment decreased WR21 and A253 cell viability and the absolute number of viable cells (Fig. 3A–C). The IL-10Rα−positive A253 cells were more sensitive to recIL-10 than the IL-10Rα−negative WR21 cells, as evidenced by reduced cell viability with increases in dead cells at an IL-10 concentration of 12.5 ng/ml (Fig. 3A–C). IL-10 treatment increased the number of dead cells for both cell lines.

In the following experiments, cells were treated with 50 ng/ml recIL-10 if not otherwise implicated. Because IL-10 can enhance invasion-associated molecules such as MMP-2 and MMP-9 in glioma cells [22], we tested cell migration in control and IL-10-treated cells. IL-10 treatment did not affect cell migration as determined using a scratch test assay (Fig S1A).

Cell viability is defined by how fast cells divide over time, exit the cell cycle, or induce cell death. Because IL-10 prevents the upregulation of the G1 cyclins D2 and D3, proteins necessary for entry and progression through the G1 phase of the cell cycle in T cells [23], cell cycle-associated genes were examined. The expression of cell cycle genes *p21* or *p27* did not change after IL-10 exposure for 24 h (Fig. S 1B). *Cyclin D* expression was lower in IL-10-treated compared to control A253 SGC cells (Fig. 3D) and showed a significant increase in A253 SG cells in G0/G1-arrest as determined by flow cytometrical analysis (Fig. 3E). No difference in the cell cycle distribution was found in IL-10-treated WR21 compared to control cells (Fig. 3E). These data suggest that IL-10 blocked cell cycle

progression and proliferation in A253 SGC cells.

2.4. IL-10 enhances ROS production

Cells exit the cell cycle in response to metabolic stress. The MTT assay was employed to further understand the IL-10-mediated effects on proliferation. The MTT cell proliferation assay measures the cell proliferation rate but is also sensitive to changes if metabolic events lead to apoptosis or necrosis. In IL-10-treated A253 cells, less yellow tetrazolium MTT was generated (Fig. 4A). To elucidate whether IL-10 hindered cancer cell proliferation by instigating a metabolic switch, we measured total reactive oxygen species (ROS) production in human A253 and mouse WR21 cells after IL-10 treatment. ROS production was determined by quantifying DCFH-
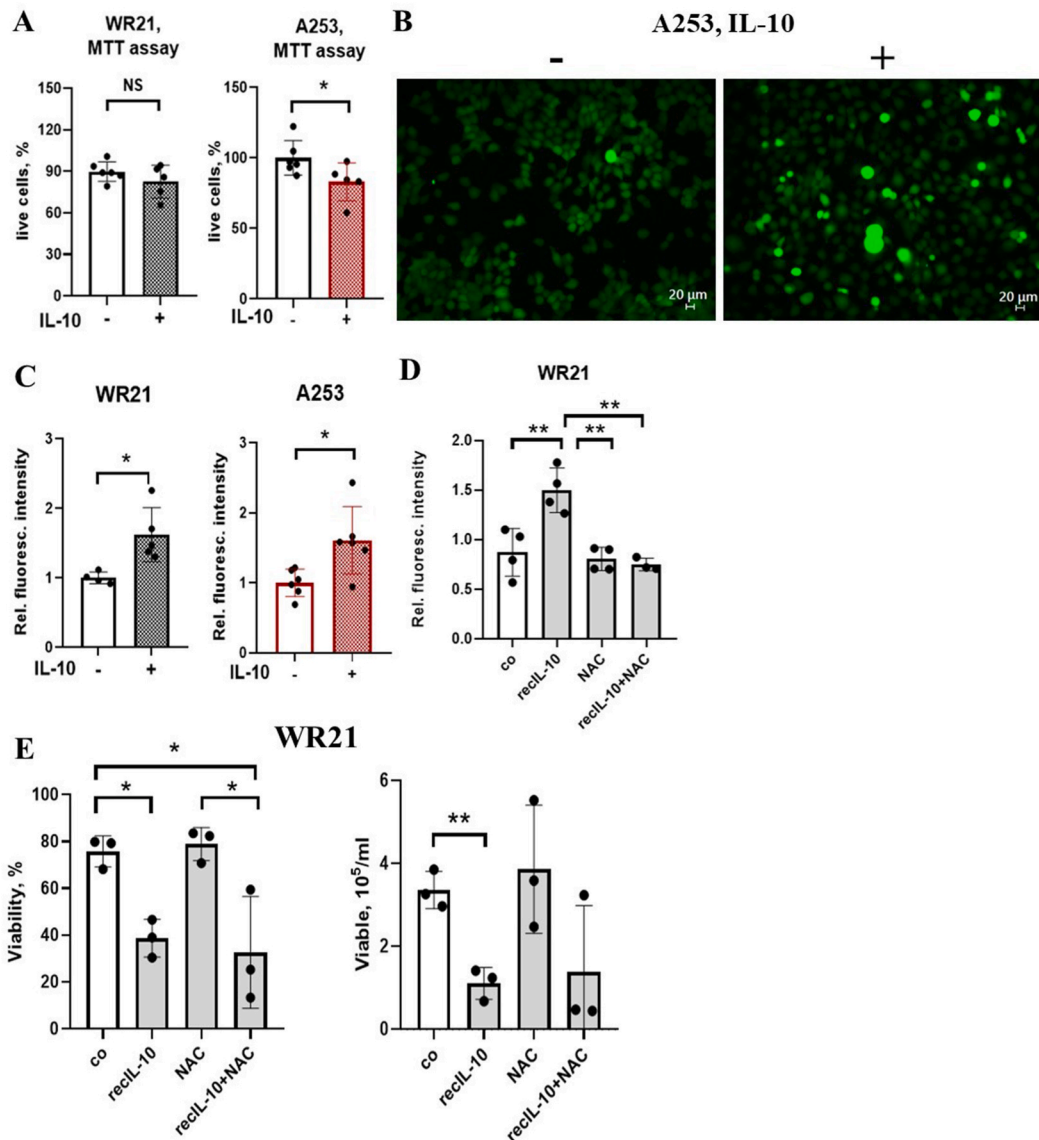

Fig. 4. IL-10 treatment augmented ROS generation, which does not have an impact on SGC cell viability A. The relative optical density of the MTT assay depicts the response of WR21 and A253 cells treated with and without recIL-10 (n = 6/group) B. Representative images of fluorescent 2′,7′-dichlorodihydrofluorescein diacetate (DCFH-DA)-stained control and IL-10-treated WR21 and A253 cells after a 24 h culture period. Bright-green fluorescence indicates ROS-producing cells. Scale bar = 20 μm. C. ROS production was determined by quantifying DCFH-DA fluorescence with normalization to total protein in control- and IL-10-treated cells (n = 6/group). D. Determination of the ROS production by quantifying DCFH-DA fluorescence with normalization to total protein in control, IL-10-, N-acetyl-ʟ-cysteine (NAC)-, and IL-10 + NAC-treated cells (n = 4/group). E. The viability rate and absolute number of viable WR21 cells in control, IL-10-, NAC-, and IL-10 + NAC-treated cells were determined by trypan blue exclusion (n = 3/group). *p < 0.05, **p < 0.01 using two-way ANOVA or Student's t-test with mean and SD depicted. (For interpretation of the references to colour in this figure legend, the reader is referred to the Web version of this article.)
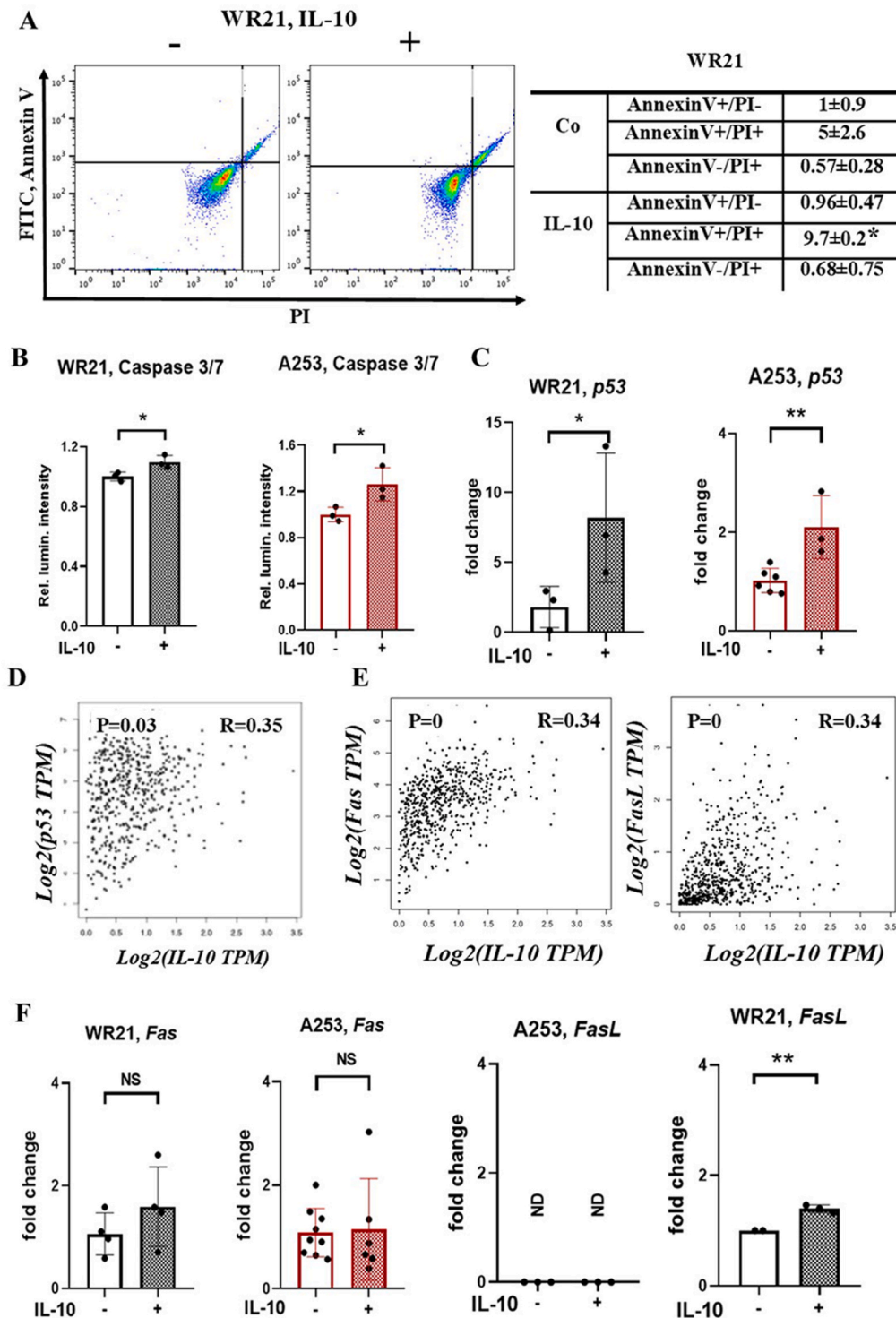
Fig. 5. IL-10 induces SGC cell apoptosis and Fas upregulation. A. Flow cytometric analysis of early and late apoptosis in IL-10-treated or control WR21 cells. Means represent two independently performed experiments. The left panel shows FACS plots of control and IL-10 treated cells stained with Annexin V-FITC and PI. The right panel shows the statistical analysis of 3 independent experiments run in duplicate. B. Caspase 3/7 activity in IL-10-treated and control cells was assayed after a 24-h incubation period using the Caspase 3,7 activity assay. The signals were normalized to control samples (n = 3/group). C. Fold change in *p53* expression of control or recIL-10-treated WR21 and A253 cells as determined by qPCR. Data were analyzed using the relative quantification method with normalization to β-actin and relative to controls. Each sample was analyzed at least in triplicate (each dot representing one cell sample), and the average fold change was determined. D. Pair-wise gene expression correlation analysis of

IL-10 and *p53* for given TCGA and GTEx expression data sets, using Pearson correlation analysis. E. Pair-wise gene expression correlation analysis of *IL-10* and *Fas*, *IL-10* and *FasL*, for given TCGA and GTEx expression data sets, using Pearson correlation analysis (source Gepia website). F. Fold change in *Fas* and *FasL* expression of control or recIL-10-treated WR21 and A253 cells. Data were analyzed using the relative quantification method with normalization to *β-actin* and relative to controls. Each sample was analyzed at least in triplicate (each dot representing one cell sample), and the average fold change was determined. *p < 0.05, **p < 0.01 using two-way ANOVA or Mann-Whitney test with mean and SD depicted.

DA fluorescence with normalizing total protein in control- and IL-10-treated cells. RecIL-10 increased total ROS production when normalized to total cell lysate protein in both cell lines (Fig. 4B and C). In line with the idea that IL-10 induces ROS, treatment with the ROS scavenger N-acetylcysteine (NAC) suppressed ROS generation after IL-10 (Fig. 4D). However, NAC could not impede the IL-10-induced reduction in WR21 cell viability (Fig. 4E), indicating that pathways other than ROS might be responsible for the IL-10-mediated inhibition of cell proliferation. The transcription factor NRF2 controls the expression of antioxidant genes, thereby protecting cells from oxidative stress and, indirectly, from ROS [24]. IL-10 treatment did not alter the expression of the oxidative stress protector NRF2 in WR21 cells (Fig. S1C). These data established that IL-10 treatment enhances ROS production. However, treatment with the antioxidant NAC could not reverse IL-10-mediated cell growth inhibition and cell death.

2.5. IL-10 causes SGC apoptosis and p53 upregulation

Since decreases in cell viability can be due to enhanced cell death, we next determined apoptosis by flow cytometry. RecIL-10-
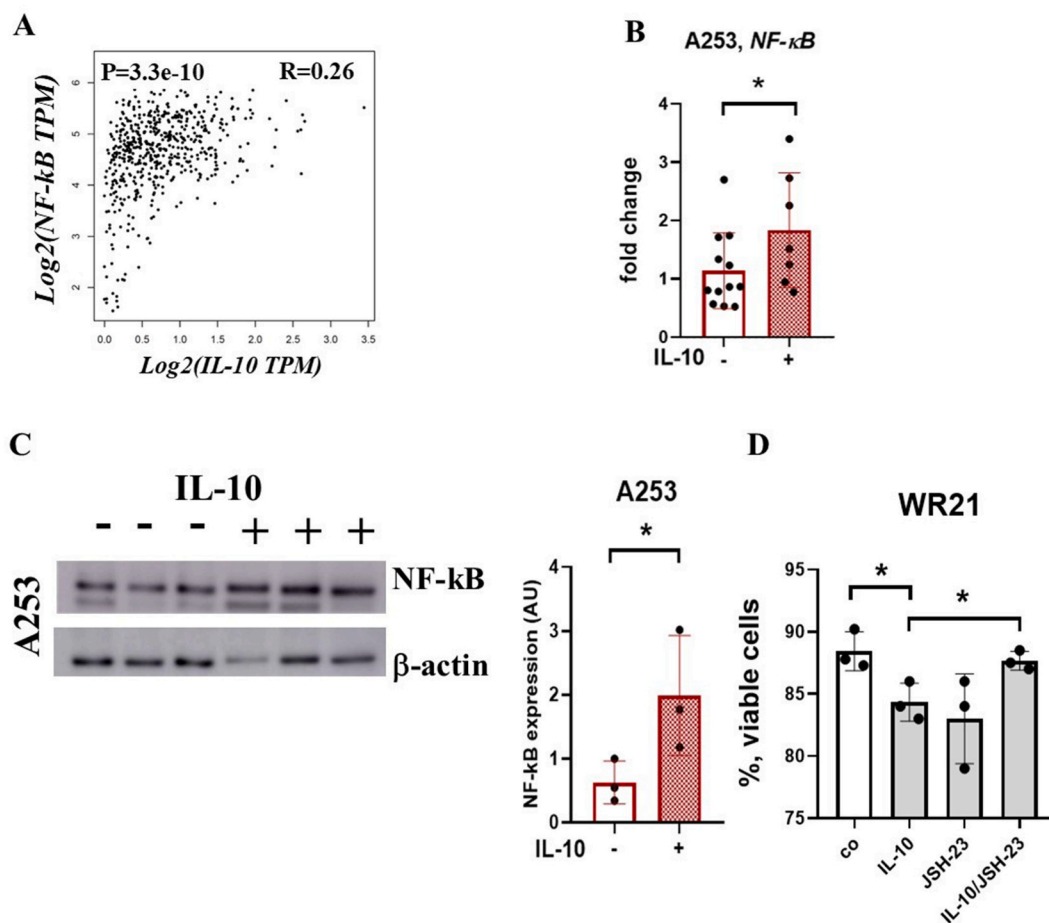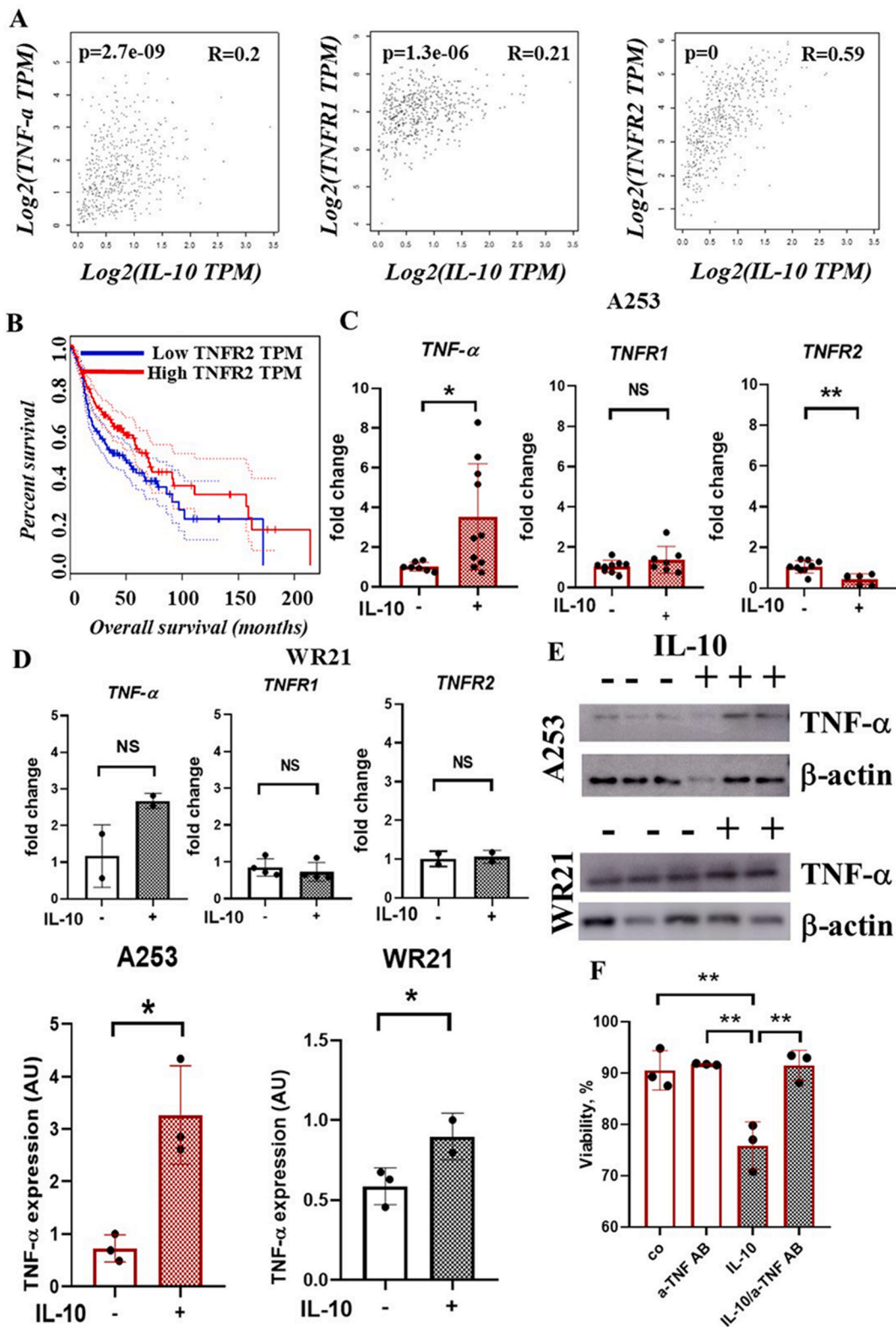

Fig. 6. IL-10 reduces cell viability through the induction of NF-kB signaling A. Pair-wise gene expression correlation analysis of *IL-10* and *NF-kB* for given TCGA and GTEx expression data sets, using Pearson correlation analysis. B. Fold change in *NF-kB* expression of control or recIL-10-treated A253 cells. Data were analyzed using the relative quantification method with normalization to *β-actin* and relative to controls. Each sample was analyzed at least in triplicate (each dot representing one cell sample), and the average fold change was determined. C. Representative Western blot (left panel) and relative band intensity (right panel) of NF-kB and β-actin (internal control) in A253 cells treated with or without IL-10 were calculated by normalizing β−actin to corresponding controls (uncropped Western blot images as Fig. S2A). D. Viability of murine WR21 cells treated with recIL-10, the NF-kB inhibitor JSH-23 (30 μM), alone and in combination after a 24-h culture period as determined by trypan exclusion (n = 3/group).

(caption on next page)

Fig. 7. IL-10-mediated impaired cell viability is dependent on TNF-α A. Pair-wise gene expression correlation analysis of *IL-10* and *TNF-α*, *IL-10* and *TNFR1*, *IL-10* and *TNFR2* for given TCGA and GTEx expression data sets, using Pearson correlation analysis. B. Kaplan-Meier plots showing the overall survival of HNSC patients with high (red line) and low (blue) *TNFR2* mRNA expression (TNFR2 Logrank p = 0.0077, HR(high) = 0.7, p(HR) = 0.0079, n(high) = 259, n(low) = 259). Patient stratification according to their *TNFR2* levels was determined using GEPIA datasets http://gepia. cancer-pku.cn/. TPM, transcripts per million. C. Fold changes in *TNF-α*, *TNFR1*, and *TNFR2* expression as determined by qPCR in A253 cells treated with/without recIL-10. Expression of the target gene was normalized to *β-actin* expression in the same samples. Fold change in gene expression was normalized to the expression in the control samples. D. Fold changes in *TNF-α*, *TNFR1* and *TNFR2* expression as determined by qPCR in murine adenocarcinoma WR21 cells treated with/without recIL-10. Expression of the target gene was normalized to *β-actin* expression in the same samples. Fold change in gene expression was normalized to the expression in the control samples. E. Representative Western blots of TNF-α and β-actin (internal control) (upper panel) in IL-10-treated and control A253 and WR21 cells. The relative band intensity (lower panel) was calculated by normalizing β−actin to corresponding controls (uncropped Western blotting images in Sup Figs. S2B and S2C). F. Viability of human A253 cells after treatment with anti-human TNF-α AB, recIL-10, alone or in combination. The number of cells was determined after a 24-h culture period by trypan exclusion (n = 3/group).*p < 0.05 using two-way ANOVA or Mann-Whitney test with mean and SD depicted. (For interpretation of the references to colour in this figure legend, the reader is referred to the Web version of this article.)

treated WR21 cells had almost twice the number of late apoptosis-indicating AnnexinV+/PI+ cells compared with the control group. Meanwhile, early apoptotic Annexin V+/PI- cells were low after treatment with recIL-10 (Fig. 5A).

Apoptosis can be driven by the upregulation of pro-apoptotic proteins, like caspases. A significant increase in the production of active caspase 3/7 was detected in WR21 adenocarcinoma and epidermoid A253 SG carcinoma cells after 24 h of recIL-10 treatment (Fig. 5B). Our data indicate that IL-10 induces apoptosis on SGC cells that involves the apoptosis-executioner caspase-3.

The tumor suppressor p53 is frequently mutated in cancers but rarely in HNSCs. p53 is activated in response to metabolic stress, which can lead to cell cycle arrest, a program that triggers apoptosis [25]. We next determined p53 expression after IL-10 stimulation. RecIL-10 treatment enhanced *p53* expression at transcript levels in A253 and WR21 SGCs (Fig. 5C) and positively correlated with p53 in human HNCS samples (Fig. 5D).

2.6. IL-10 upregulates FasL in SGC cells and correlates to human Fas expression

Our findings in SGC cell lines suggest a potential association between IL-10 and p53. p53 regulates genes associated with the extrinsic apoptotic pathway, such as Fas ligand (FasL) [26]. Therefore, we next performed a Pearson correlation analysis of human HNCS patient samples using the bioinformatic tool GEPIA for IL-10 and Fas/FasL. As shown in (Fig. 5E), IL-10 positively correlated with Fas (Pearson correlation = 0.34 P-value = 0) and FasL expression (Pearson correlation = 0.34 P-value = 0) in human HNCS patient data sets.

We next tested *Fas* and *FasL* expression after Il-10 treatment. *Fas* expression did not change in IL-10-treated WR21 and A253 cells compared to controls (Fig. 5F). In contrast, our investigation showed an upregulation of the pro-apoptotic gene *FasL* after IL-10 treatment in WR21 cells. No *FasL* expression was detectable in A253 cells (Fig. 5F). These data indicated that extrinsic apoptotic pathway activation could contribute to IL-10-mediated apoptosis.

2.7. NF-kB contributes to IL-10-mediated growth inhibition

Fas signaling activates NF-kB pathways [27]. According to the bioinformatic tool GEPIA, IL-10 positively correlated with NF-kB in a dataset of HNSC patients (Fig. 6A). We found that *NF-kB* transcript and protein levels increased in IL-10-treated compared to control A253 cells (Fig. 6B–C).

To elucidate the functional consequences of IL-10 in the absence of NF-kB, we treated WR21 cells with IL-10 in the presence or absence of the NF-kB inhibitor JSH-23 (Fig. 6D). Treatment with recIL-10 but not the NF-kB inhibitor JSH-23 decreased the absolute number of viable WR21 cells (Fig. 6D). NF-kB inhibition reversed the IL-10-mediated SGC growth inhibition. These data indicate that NF-kB, at least in part, might contribute to IL-10-mediated SGC growth inhibitory effects.

2.8. IL-10-mediated SGC proliferation inhibition is dependent on TNF-α

IL-10 deficient enteroids show a defective NF-kB activation, with dysregulated gene expression of NF-kB downstream targets, such as TNF-α [28]. The ligation of TNFR1 by soluble TNF activates NF-kB and MAPK signaling and apoptosis pathways [29]. In patients with HNSC tumors, a positive correlation between NF-kB and TNF-α was observed (Fig. S1D). We hypothesized that IL-10 enhances *TNF-α* expression in IL-10^{low} expressing SGC cells. Pearson correlation analysis of data from HNSC patients revealed a positive correlation between *IL-10*, *TNF-α*, *TNFR1*, and *TNFR2* (Fig. 7A), suggesting that high *IL-10* correlated with high TNF-α, TNFR1 and TNFR2 expression.

High *TNFR2* expression in HNSC tumor tissues indicated better survival in HNSC patients (Fig. 7B). No change in *TNFR1 and TNFR2* expression was found in both SGC cell lines (Fig. 7C and D). IL-10 treatment enhanced TNF-α transcript and/or protein levels in A253 and WR21 cells compared to controls (Fig. 7C–E). These data suggest that IL-10 treatment enhanced TNF-α protein expression in A253 and WR21 SGC cells.

Given the increased TNF-α expression following IL-10 treatment, we sought to determine if blocking TNF-α would reverse IL-10-mediated apoptosis. Rec IL-10 impaired A253 cell viability (Fig. 7F) and enhanced the number of PI + cells (data not shown). Notably,

the impaired IL-10-mediated viability was rescued upon the addition of neutralizing antibodies against TNF-α (Fig. 7F), indicating that IL-10 drives SGC cell apoptosis through TNF-α.

3. Discussion

While the anti-inflammatory role of IL-10 has been widely studied in cancers [30,31], the role of IL-10 in HNSC and SGCs is unclear. We identified IL-10 as a crucial anti-tumor cytokine in SGCs. We delineated a mechanism by which IL-10 directly causes SGC tumor cell apoptosis by activating proapoptotic pathways via TNF-α as shown using neutralizing antibodies. Mechanistically, IL-10 treatment reduces total NF-kB, which might impede cell survival, ultimately leading to caspase-3/7-mediated apoptosis (Graphic abstract). We also observed enhanced ROS production and p53 and Fas expression in SGC cells that might further promote the anti-tumor effects of IL-10 on SGC cells. Finally, we showed that IL-10 upregulated NF-kB expression in SGC cells, contributing to growth inhibition.

Consistent with previous findings [32], we found diminished expression of immunoreactive IL-10 in human SGC ductal cells. The efficacy of IL-10 signaling hinges upon the expression of IL-10Rs. Elevated IL-10 and IL-10Rα expression levels in tumor tissues indicated better survival in HNSC patients. This observation aligns with a recent study reporting high IL-10 expression in the immune-high reaction group of patients with SG epidermoid carcinoma, correlating with a favorable prognosis [33]. We confirmed the expression of IL-10 and its receptors IL-10Rα/-β in human A253 SG epidermoid carcinoma cells. In contrast, the murine SGC cell line, WR21 cells, lacked IL-10 and IL-10Rα but expressed IL10Rβ.

Encouraged by IL10R expression in SGC cells, we explored the responsiveness of SGC cells to IL-10. Drawing on findings from murine pancreatic cancer models [34] and IL-10Rα-expressing lymphoma cells [35], our study revealed impaired A253 and WR21 SGC tumor cell viability and growth upon exposure to recIL-10. Also, treatment with recIL-10 upregula*ted IL-10* and *IL-10Rα* expression by A253. IL-10 expression correlated to SG tumor phenotypes with better overall survival (Fig. 1B) [33]. The observed IL-10 upregulation after IL-10 treatment in A253 cells might be due to an autocrine positive feedback loop previously described whereby exogenous IL-10 upregulates CD64 (Fc-gamma receptor 1) expression, and subsequent CD64 ligation enhances IL-10 transcription and translation [36]. CD64 is highly expressed in SG in normal conditions by SG macrophages, T cells, mucous, and serous glandular cells, as well as by epidermoid carcinoma A253 cells (transcription level 0.5 nTPM), as retrieved from the Human Protein Atlas [37]. However, further studies are needed to determine the involvement of CD64 in autocrine IL-10 amplification in SGC cells.

We demonstrated that IL-10 stimulation induces ROS production in SGC cells. Although ROS can lead to apoptosis in response to death-inducing ligands such as TNF-α and Fas signaling in SGC cells [38], treatment with NAC could reverse IL-10-induced ROS production but not apoptosis.

p53 is frequently mutated in cancers, including mucoepidermoid carcinoma (MEC), but rarely in HNSCs, and ways to enhance its expression have been proposed as treatment options for HNSCs. We demonstrated that IL-10 exposure enhanced p53 expression in SGC cells, as reported in hepatic stellate cells [39]. A recent study showed that p53 activation, as achieved by treating MEC cells with the mouse double minute 2 (MDM2) inhibitor MI-773, which activates p53 signaling by disrupting the binding between MDM2 and p53, induces MEC cancer stem cell (CSC) apoptosis by reducing CSC self-renewal via Bmi-1, causing cell differentiation [40]. Future studies will be necessary to evaluate whether IL-10 in SGC cells can influence CSC fate and might have targeted CSCs.

DNA damage, and as we showed here, IL-10 treatment can target both the NF-kB and the p53 pathways. p53 is activated in response to cellular damage, initiating cell cycle arrest and apoptosis. IL-10-treated SGC cells accumulated in the G1 phase and did not progress into the S phase of the cell cycle, accompanied by downregulation of the cell cycle regulator cyclin D, as previously shown during hepatocyte carcinoma progression [41]. The G2/M checkpoint, positioned between the G2 and M phases, prevents cells with damaged DNA from progressing through the cell cycle.

The contribution of NF-kB to SGC cell fate is more complex. NF-kB counteracts death signaling at crucial crosspoints in the extrinsic and intrinsic death pathways [42], including the pro-apoptotic function of p53 [43]. Studies demonstrated that epithelium-derived IL-10 in the intestinum functions as a positive regulator of NF-kB [28]. We found that IL-10 addition enhanced NF-kB expression in SGC cells. A recent study in IL-10 deficient mice showed that upon TNF injection, tissue from the small intestine showed upregulation of NFκB p65[RelA] activity, which was diminished in IL-10 deficient mice and correlated with reduced levels of TNF-α expression [44]. We identify TNF-α as a critical mediator of IL-10-mediated SGC apoptosis as neutralizing antibodies against TNF-α restored IL-10-driven SGC viability. Notably, IL-10 can enhance its expression in SGC cells, analogous to an autoregulatory amplification loop observed in melanoma cells [45]. An alternative hypothesis is that IL-10, potentially via TNF-α upregulation, enhances IL-10 expression, thereby establishing an autocrine amplification loop akin to observation in macrophages [46,47].

Given that IL-10's anti-proliferative effects as a single treatment might not be sufficient to control SGC tumor growth, IL-10 treatment in combination with myelosuppression (chemotherapy and irradiation) should be considered. We found that recIL-10 enhanced NF-kB expression and impaired cell viability in IL-10^{low}-expressing SGC cells. Intrinsic NF-kB activation triggers SGC cell resistance to ionizing radiation [48]. Considering NF-kB's known contribution to irradiation resistance and the potential of IL-10 to enhance NF-kB activity, further investigations are necessary to explore whether IL-10 cotreatment with myelosuppression can enhance treatment efficacy.

IL-10 is an ideal drug to control SGC cell survival as it can induce apoptosis and activate p53. Pegylated IL-10 given as monotherapy showed objective tumor responses in 4 of 15 patients with intermediate to poor risk in renal cell cancer without inducing autoimmune toxicities [49]. While cytokine treatments' major concerns include toxicity and tolerability, the Naing study showed that although adverse events occurred, they were manageable and reversible on dose interruption or reduction.

The Fas-FasL system has emerged as a prognostic factor for SGC disease severity [50]. Our data revealed that IL-10 enhanced FasL expression in murine WR21 SGC cells. This system is used by CD8^{+} T cells and natural killer cells to eliminate cancer cells, while tumor

cells can also employ this system to counterattack tumor-infiltrating immune cells. FasL upregulation after IL-10 could arm SGC tumor cells to eliminate tumor-infiltrating immune cells, such as T cells in the circulation and at the tumor site [50], contributing to the immune escape of HNSCs. Our study has not tested this aspect of IL-10 on the immune response. The dual role of Fas-FasL signaling, acting not only on tumor killing and targeting T lymphocytes, underscores the need for careful consideration of IL-10 administration and is imperative for developing better-targeted anti-cancer therapy.

In summary, this study provides new insights into the regulatory role of IL-10 in SGC cancer cells. Our results laid the groundwork for subsequent preclinical studies using tumor-targeted IL-10 approaches alone or combined with established myelosuppressive drugs for treating HNSC and SGC tumor patients.

3.1. Limitations of the study

The current study found that IL-10 suppresses SGC cell proliferation and enhances apoptosis by inducing TNF-α expression *in vitro*. Although we have shown that TNF-α-signaling can prevent IL-10-driven cell proliferation, it is unclear whether this is the only pathway modulated by IL-10 on SGC cells.

Finally, whereas this study showed IL-10 effects on SGC cells *in vitro*, future studies will be required to determine the IL-10-driven effects on the tumor microenvironment. It will be important to demonstrate whether the tumor environment can compensate for IL-10 deficiency in SGC tumor cells in vivo, e.g., using IL-10-deficient mice. Another limitation is that while this study investigated the direct effect of IL-10 on SG cancer cells, the *in vitro* study conditions did not consider the essential immunomodulatory functions of IL-10 involved in cancer immunity in vivo. These studies would require injecting tumor cells with control and IL-10 overexpressing SGC cancer cells into wild-type, IL-10, or IL10 receptor-deficient mice.

4. Materials and methods

4.1. Primary MM patient samples

Salivary gland operative materials were obtained from patients, and healthy donors provided written informed consent before sample collection. The study protocols were per the Declaration of Helsinki and approved by the institutional review board at Poltava State Medical University, protocol number 07.04/122 from January 19, 2023.

4.2. HE and IL-10 staining of human tissue sections

Salivary glands were fixed in 4 % paraformaldehyde, and paraffin blocks were generated. 3um thick sections were cut. Tissue sections were stained with hematoxylin and eosin (HE). The diagnosis was determined according to the histopathological findings in Supplementary Table 1. Furthermore, tissue sections were blocked and stained with the primary mouse monoclonal anti-human IL-10 (E−10) antibody (Cat. sc-8438, Santa Cruz Biotechnology, INC) dilution 1:100 overnight at 4 °C followed by staining with secondary antibody Goat, Anti-mouse Ig (Dako, E0433, LOT 00095329) 1:200. Nuclei were counterstained with hematoxylin (Cat. 4987481295841, Wako). Images were taken using an Olympus BX53 light microscope.

4.3. Drugs and cytokines

Recombinant human IL-10 (Cat. 571004, BioLegend, San Diego, California, USA), Recombinant mouse IL-10 (Cat. 575804, Bio-Legend, San Diego, California, USA), anti-human TNFa neutralizing antibody (Biotechne, #AF-210-NA), recombinant human TNFa (Biotechne, #210-TA), N-acetyl-ʟ-cysteine (NAC; Cat. A7250, Sigma-Aldrich, USA), JSH-23, (NF-kB Activation Inhibitor II (Cat. CAS 749886-87-1, Calbiochem, USA; IC$_{50}$ of 7.1 μM in RAW 264.7 cell line. JSH-23 does not show significant cytotoxic effects on the RAW 264.7 cells at <100 μM [51].) All were reconstituted as recommended by the manufacturer and added to cultures at the indicated concentrations.

4.4. Cell lines

The basic media for A253 human submandibular salivary glands carcinoma cells (Cat. HTB-41, ATCC, Virginia, USA) was McCoy's 5A (Modified) Medium (Cat. 16600082, Gibco); for THP-1 acute monocytic leukemia monocytes (Cat. TIB-202, ATCC, Virginia, USA) was RPMI-1640 medium (Cat. 11875093, Gibco) with 0.05 mM of 2-mercaptoethanol, for U-937 human histiocytic lymphoma cells (Cat. CRL-1593.2, ATCC, Virginia, USA) was RPMI-1640 medium (Cat. 11875093, Gibco); for HL-60 human promyeloblast cells (Cat. CCL-240, ATCC, Virginia, USA) was IMDM (Cat. 12440053, Gibco), HUVEC human umbilical venule endothelial cells (Cat. CRL-1730, ATCC, Virginia, USA) was F−12K Medium (Cat. 30−004, ATCC) supplemented with heparin (Cat. H3393, Sigma) and ECGS (Cat. CB-40006, Fisher Scientific); for HEK human kidney embryonic cells (Cat. CRL-1573, ATCC, Virginia, USA) was MEM (Cat. 30−003, ATCC); for WR21 mouse submandibular salivary gland adenocarcinoma cells (Cat. CRL-2189, ATCC, Virginia, USA) was D-MEM medium (Cat. 044−29765, FUJIFILM Wako Pure Chemical Corporation). Aside from the basic medium, all media contained 10 % FBS (Cat. FB-1380, BioSera) and 1 % Penicillin-Streptomycin (P/S; Cat. 15140122, Gibco).

4.5. Cell proliferation or cytotoxicity assay after drug-addition

Cells were cultured in triplicate at 4×10^4/ml for WR21 and 1×10^5/ml for A253 cells in 6-well plates. Following cell adherence, rec. IL-10 alone or combined with the NF-kB inhibitor JSH-23 (30 μM) were added to the cultures. IL-10 (Rec. human for A253 cells and mouse for WR21 cells) was used in concentrations 12.5, 25, and 50 ng/ml. If not otherwise indicated, rec. IL-10 was added to cultures at a concentration of 50 ng/ml. After 24 h of incubation, cells were trypsinized with trypsin-EDTA solution (Cat. 205–20255, WAKO, Japan). A trypan blue exclusion test was used to determine cell viability. Cells were counted using CellDrop (DeNovix, USA).

For measuring cytotoxicity, WR21 and A253 cells were cultured with the indicated IL-10 concentrations at a cell density of 4×10^3/ well and A253 1×10^4/well using 96-well plates, respectively. 24 h later, the MTT reagent from the Cell Counting Kit-8 (Cat. CK04, Dojindo, Japan) was added. Absorbance was measured at the wavelength of 450 nm by a microplate reader against 650 nm SpectraMax ABS/ABS Plus (Molecular Devices, USA) after an incubation period of 1.5 h at 37 °C, 5 % CO_2.

WR21 cells were cultured in triplicates at 4×10^4/ml in 6-well plates. Following cell adherence, rec. mouse IL-10 (50 ng/ml) alone or combined with NAC (5 μM) were added to the cultures. After 24 h of incubation, cells were trypsinized using a trypsin-EDTA so-lution (Cat. 205–20255, WAKO, Japan). A trypan blue exclusion test was used to determine cell viability. Cells were counted using CellDrop (DeNovix, USA).

A253 cells ($1.5x10^5$/ml) were plated in 6-well plates. After cells had adhered, the mouse rec. IL-10 (50 ng/ml), rec. TNFa 10 ng/ml (Biotechne, #210-TA) or anti-human TNFa neutralizing antibody 400 ng/ml (anti-TNF-AB; Biotechne, #AF-210-NA) were added alone or in combination as indicated. After a 24-h culture period, cells were trypsinized, and a trypan blue exclusion test was used to determine cell viability. Cells were counted manually.

4.6. Migration assay

Cultures were initiated with 1×10^5 cells/ml for WR21 and 2×10^5 cells/ml for A253 in standard medium using 12-well plates. When cells reached confluency, the medium was removed, and cells were washed once with PBS. A scratch was made, and the scratch border was marked on the plates in the middle of the well using a 100ul pipet tip. Following two additional PBS washes, fresh medium with 2 % FBS (FBS-reduced) was added to the wells, and cell treatment was started. The medium was supplemented with 50 ng/ml of recIL-10. The all-in-one Fluorescence Microscope, BZ-X series (Keyence, USA), was used to take a photo of the initial scratch size, and again after 24 h of incubation at 37 °C, 5 % CO2. Images were analyzed using ImageJ software, and the percent of migration was measured as the cell-free surface width of the scratch after 24 h of treatment. The initial surface width of the scratch is 100 %.

4.7. Caspase 3/7 assay

A253 and WR21 cells were added to 96 chimney well cell microplates (Cat. 655083, Grainer, Germany) at a concentration of 1500 and 2000 cells per well, respectively. Cells were cultured for 20 h with/without rec IL-10 (50 ng/ml) at 37 °C, 5 % CO_2. Culture plates were stored at room temperature for 30 min. Then, the mix of the Caspase-Glo 3/7 substrate and buffer (Cat. G810C, Promega, USA) was added to the medium at a ratio of 1:1. After 1.5 h at RT, luminescence was measured with the FlexStation3 Molecular Devices and the relative luminescence intensity was calculated according to the manufacturer's protocol.

4.8. Cell cycle

Single cells were harvested in PBS plus 2 % FBS buffer, washed, and spun at $300 \times g$ for 5 min 70 % ethanol was added dropwise for cell fixation, and the samples were incubated for 60 min on ice. After two PBS washes, samples were incubated with RNase A (50 μl; of 100 μg/ml stock solution) (Cat. EN0531, Thermo Scientific™) for 1 h. Cells were stained with propidium iodide (PI; 1ug/ml; Cat. 5135, Tocris Bioscience) [52]. Stained cells were analyzed using a FACSCelesta™ Cell Analyzer, BD Biosciences. FlowJO software was used to analyze the data.

4.9. Apoptotic assay

A253 ($5x10^4$/ml) and WR21 cells ($1x10^5$/ml) were plated in 6-well plates in the presence or absence of recIL-10 (50 ng/ml). After a 20-h culture period, cells were trypsinized, washed twice, resuspended with the buffer from the annexin V staining kit, and stained with Annexin V and PI for 20 min (Cat. 556547, BD Pharmingen™ FITC Annexin V Apoptosis Detection Kit I). Stained cells were analyzed by FACSCelesta™ Cell Analyzer BD Biosciences. FlowJO software was used for FACS plot analysis.

4.10. Detection of total reactive oxygen species (ROS)

Cultured WR21 and A253 cells were stained with 2′,7′-Dichlorodihydrofluorescein diacetate (Cat. D6883, 0000143276, Sigma-Aldrich, St. Louis, USA) [53]. Images of stained cells were taken with the green fluorescent protein channel on an All-in-One Fluo-rescence Microscope, BZ-X series (Keyence, USA). For total ROS quantification, cells were lysed using RIPA Lysis and Extraction Buffer (Cat. 89900, Thermo Scientific). After centrifugation, 100 μl of the cell lysate supernatants were transferred into a black 96-well plate. The fluorescence intensity was measured using a fluorescence microplate reader at an excitation wavelength of 485 nm and an emission wavelength of 530 nm using the FlexStation3 Molecular Devices. ROS data was normalized to the total protein concentration

in each sample.

Quantification of messenger RNA (mRNA) expression by reverse-transcription-polymerase chain reaction (PCR).

Total RNA was extracted using RNA TRIzol (Invitrogen), and cDNA was generated according to the manufacturer's protocols using the high-capacity cDNA reverse transcription kit (Cat. No. 4368814, Applied Biosystems). cDNA (10 ng) was used as a template for each PCR amplification using specific forward and reverse primer pairs listed in Table 2. For quantitative real-time PCR, PCR mixtures were prepared using SYBR Premix Ex *Taq*II (Takara) containing 0.2 mM of each primer, and amplification reactions were performed. Gene expression levels were determined by measuring the intensity of SYBR Green fluorescence using the QuantStudio 3 qPCR System (Applied Biosystems™).

4.11. Western blotting

Cell lysates for WB preparation. Cells were lysed with RIPA Lysis and Extraction Buffer (Cat. 89900, Thermo Scientific) with Protease Inhibitor Cocktail (Cat.5871, Cell Signaling Technology) 100:1, incubated on ice for 5 min and collected into the tubes, then stored until use at $-80\,^{\circ}$C. Before usage, protein concentrations were measured in cell lysates with the earlier method, and then 20 µg of protein was loaded into each well. Before loading, cell lysates were mixed with 5x Laemmli Sample Buffer (Cat. 1610747, Bio-Rad) and heated for 5 min at 98 °C. According to the manufacturer's instructions, Bio-Rad's tank blotting cells and PowerPac™ Universal Power Supply (Bio-Rad) equipment were used for western blotting. M: Molecular marker Dual Color (Cat. 1610374, Bio-Rad) was used (10–250 kD). All protein concentrations in each sample were normalized to β-actin.

Primary AB included Mouse anti-β-actin AB (Cat.643801, clone 2F1-1, BioLegend) 1:1000; Goat polyclonal TNFalpha (Cat.AF-210-NA, Biotechne) 1.5 µg/mL, Rabbit polyclonal anti–NF–kB (Cat. sc-109, Santa Cruz) 1:200.

The appropriate secondary ABs were chosen with Goat anti-rabbit IgG-HRP (Cat. sc-2004, Santa Cruz) 1:8000, goat anti-mouse HRP-conjugated (Cat.81-6520, ZyMax™) 1:3000; rabbit anti-goat HRP-conjugated (Cat. SA00001-4, ProteinTech) 1:10000.

4.12. Bioinformatics analysis

The GEPIA RNA sequence data sets were used for analysis. Data were analyzed using the GEPIA database (Gene Expression Profiling Interactive Analysis, http://gepia.cancer-pku.cn/). For Kaplan Meier (overall survival) curves, we used a median 50 cutoff-high (%) and 50 cutoff-low (%) and a 95 % confidence interval [54].

4.13. Statistical analysis

GRAPHPAD PRISM 8.0.1 by Dotmatics was used for statistical data processing. All results were described as mean and standard deviation. For data analysis, we used a one-factor analysis of variance (one-way ANOVA) for unrelated samples and Bonferroni analysis for multiple comparisons. The difference between groups was considered statistically significant at $p < 0.05$. The difference between the two groups was determined using the Student's t-test.

Table 2
Human and mouse primers.

Target	Forward	Reverse
Human primers		
β-actin	CCAACCGCGAGAAGATGA	CCAGAGGCGTACAGGGATAG
IL-10Rβ	GGGTCGTGTGCTTGGAGG	AGCAGGTGACTCCCACTGTA
IL-10Rα	CTGCAGGGCTGGTCAGGG	CTCCAGAAAGCCCCATGGTT
IL-10	GGCACCCAGTCTGAGAACAG	ACTCTGCTGAAGGCATCTCG
TNFRα1	ACCAACGGTGGAAGTCCAAG	AGTAGTTCCTTCAAGCTCCCC
TNFRα2	CCAGTGCGTTGGACAGAAG	CACCAGGGGAAGAATCTGAGC
TNF-α	CTCTTCTGCCTGCTGCACTTTG	ATGGGCTACAGGCTTGTCACTC
NF-κB	TGAACCGAAACTCTGGCAGCTG	CATCAGCTTGCGAAAAGGAGCC
Mouse primers		
β-actin	GGCTGTATTCCCCTCCATCG	CCAGTTTGGTAACAATGCCATGT
IL-10	CGGGAAGACAATAACTGCACCC	CGGTTAGCAGTATGTTGTCCAGC
IL-10Rα	CCAAACCAGTCTGAGAGCACCT	CAGGACAATGCCTGAGCCTTTC
NF-κB	GCTGCCAAAGAAGGACACGACA	GGCAGGCTATTGCTCATCACAG
IL-10Rβ	TTTGTCGTGCTGTGGCTCAT	AGGGAAGGAGAACAGCAGAA
P21	TCGCTGTCTTGCACTCTGGTGT	CCAATCTGCGCTTGGAGTGATAG
p27	AGCAGTGTCCAGGGATGAGGAA	TTCTTGGGCGTCTGCTCCACAG
Cyclin D	GCAGAAGGAGATTGTGCCATCC	AGGAAGCGGTCCAGGTAGTTCA
Fas	CTGCGGATTCTCCTGGCTGTGAA	CAACAACCATAGGCGATTTCTGG
FasL	GAAGGAACTGGCAGAACTCCGT	GCCACACTCCTCGGCTCTTTTT
p53	GTATTTCACCCTCAAGATCC	TGGGCATCCTTTAACTCTA
TNF-α	GCCGATTTGCTATCTCATCA	GGTATATGGGCTCATACCAG
TNFRα1	ACCGTGACAATCCCCTGTAA	AGGGACGCACTCACTTTCTC
TNFRα2	TTGACACCCTACAAACCGGAA	TTTCACATATTGGCCAGGAGGA
NRF2	ACCTCTGCTGCAAGTAGCCT	TGCCTCCAAAGGATGTCAATCA

4.14. Images analysis

Images analysis was done with ImageJ software (Rasband, W.S., ImageJ, U. S. National Institutes of Health, Bethesda, Maryland, USA).

4.15. Ethics Statement

All human subjects freely gave their written informed consent to participate in the study. The study protocols were per the Declaration of Helsinki. The ethics committee (institutional review board) of Poltava State Medical University, Poltava, Ukraine (protocol reference number 07.04/122 from January 19, 2023) approved the study. The study was conducted in accordance with local legislation and institutional regulations and requirements.

Data availability

Data are available in the article and its supplementary materials.

CRediT authorship contribution statement

Maksym Skrypnyk: Writing – original draft, Investigation, Formal analysis, Data curation, Conceptualization. **Tetiana Yatsenko:** Supervision, Methodology, Formal analysis, Data curation. **Oleksandra Riabets:** Data curation. **Margarita Skikevych:** Funding acquisition. **Taro Osada:** Methodology, Data curation. **Morikuni Tobita:** Funding acquisition. **Satoshi Takahashi:** Funding acquisition. **Koichi Hattori:** Funding acquisition. **Beate Heissig:** Investigation, Funding acquisition, Conceptulaization.

Declaration of competing interest

The authors declare that they have no known competing financial interests or personal relationships that could have appeared to influence the work reported in this paper.

Appendix A. Supplementary data

Supplementary data to this article can be found online at https://doi.org/10.1016/j.heliyon.2024.e31777.

References

[1] T. Ettl, S. Schwarz-Furlan, M. Gosau, T.E. Reichert, Salivary gland carcinomas, Oral Maxillofac Surg 16 (2012) 267–283, https://doi.org/10.1007/s10006-012-0350-9.

[2] K.Y. Zhan, S.F. Khaja, A.B. Flack, T.A. Day, Benign Parotid tumors, Otolaryngol Clin North Am 49 (2016) 327–342, https://doi.org/10.1016/j.otc.2015.10.005.

[3] I.A. Vathiotis, J.M. Johnson, A. Argiris, New systemic Therapies in salivary gland cancer, in: Critical Issues in Head and Neck Oncology, Springer International Publishing, Cham, 2023, pp. 327–345, https://doi.org/10.1007/978-3-031-23175-9_20.

[4] K. Wang, J.S. Russell, J.D. McDermott, J.A. Elvin, D. Khaira, A. Johnson, T.A. Jennings, S.M. Ali, M. Murray, C. Marshall, D.S. Oldham, D. Washburn, S.J. Wong, J. Chmielecki, R. Yelensky, D. Lipson, V.A. Miller, P.J. Stephens, H.S. Serracino, J.S. Ross, D.W. Bowles, Profiling of 149 salivary Duct carcinomas, carcinoma Ex pleomorphic adenomas, and adenocarcinomas, not otherwise specified reveals actionable genomic alterations, Clinical Cancer Research 22 (2016) 6061–6068, https://doi.org/10.1158/1078-0432.CCR-15-2568.

[5] C.P. Rodriguez, Q. Vicky Wu, J. Voutsinas, J.R. Fromm, X. Jiang, V.G. Pillarisetty, S.M. Lee, R. Santana-Davila, B. Goulart, C.S. Baik, L.Q.M. Chow, K. Eaton, R. Martins, A phase II trial of pembrolizumab and vorinostat in recurrent metastatic head and neck squamous cell carcinomas and salivary gland cancer, Clinical Cancer Research 26 (2020) 837–845, https://doi.org/10.1158/1078-0432.CCR-19-2214.

[6] R. Lang, D. Patel, J.J. Morris, R.L. Rutschman, P.J. Murray, Shaping gene expression in activated and resting primary macrophages by IL-10, The Journal of Immunology 169 (2002) 2253–2263, https://doi.org/10.4049/jimmunol.169.5.2253.

[7] D.S. Shouval, J. Ouahed, A. Biswas, J.A. Goettel, B.H. Horwitz, C. Klein, A.M. Muise, S.B. Snapper, Interleukin 10 receptor signaling, 177–210, https://doi.org/10.1016/B978-0-12-800267-4.00005-5, 2014.

[8] M. Oft, IL-10: master switch from tumor-promoting inflammation to antitumor immunity, Cancer Immunol Res 2 (2014) 194–199, https://doi.org/10.1158/2326-6066.CIR-13-0214.

[9] L. Shen, J. Li, Q. Liu, W. Song, X. Zhang, K. Tiruthani, H. Hu, M. Das, T.J. Goodwin, R. Liu, L. Huang, Local blockade of interleukin 10 and C-X-C motif chemokine ligand 12 with nano-delivery promotes antitumor response in murine cancers, ACS Nano 12 (2018) 9830–9841, https://doi.org/10.1021/acsnano.8b00967.

[10] K.S. Rallis, A.E. Corrigan, H. Dadah, A.M. George, S.M. Keshwara, M. Sideris, B. Szabados, αβ, Anticancer Res 41 (2021) 3247–3252, https://doi.org/10.21873/anticanres.15110.

[11] M. Hamzavi, A.A. Tadbir, G. Rezvani, M.J. Ashraf, M.J. Fattahi, B. Khademi, Y. Sardari, N. Jeirudi, Tissue expression, serum and salivary levels of IL-10 in patients with head and neck squamous cell carcinoma, Asian Pacific Journal of Cancer Prevention 14 (2013) 1681–1685, https://doi.org/10.7314/APJCP.2013.14.3.1681.

[12] A. Omran, H. Sobh, M.O. Abdalla, S. El-Sharkawy, A.R. Rezk, A. Khashana, Salivary and serum interleukin-10, C-reactive protein, mean platelet volume, and CRP/MPV ratio in the diagnosis of late-onset neonatal sepsis in full-term neonates, J Immunol Res 2021 (2021) 1–7, https://doi.org/10.1155/2021/4884537.

[13] G.M. Villarreal, J. Alcocer-Varela, L. Llorente, Differential interleukin (IL)-10 and IL-13 gene expression in vivo in salivary glands and peripheral blood mononuclear cells from patients with primary Sjögren's syndrome, Immunol Lett 49 (1996) 105–109, https://doi.org/10.1016/0165-2478(95)02490-5.

[14] J. Schnoell, L. Kadletz, B.J. Jank, F. Oberndorfer, F.F. Brkic, E. Gurnhofer, J. Cede, R. Seemann, L. Kenner, G. Heiduschka, Expression of inhibitors of apoptosis proteins in salivary gland adenoid cystic carcinoma: XIAP is an independent marker of impaired cause-specific survival, Clinical Otolaryngology 45 (2020) 364–369, https://doi.org/10.1111/coa.13509.

[15] F. Driessler, K. Venstrom, R. Sabat, K. Asadullah, A.J. Schottelius, Molecular mechanisms of interleukin-10-mediated inhibition of NF-κB activity: a role for p50, Clin Exp Immunol 135 (2003) 64–73, https://doi.org/10.1111/j.1365-2249.2004.02342.x.

[16] H. Blaser, C. Dostert, T.W. Mak, D. Brenner, TNF and ROS crosstalk in inflammation, Trends Cell Biol 26 (2016) 249–261, https://doi.org/10.1016/j.tcb.2015.12.002.

[17] D. Brenner, H. Blaser, T.W. Mak, Regulation of tumour necrosis factor signalling: live or let die, Nat Rev Immunol 15 (2015) 362–374, https://doi.org/10.1038/nri3834.

[18] M. Sisto, M. D'Amore, S. Caprio, V. Mitolo, P. Scagliusi, S. Lisi, Tumor necrosis factor inhibitors block apoptosis of human epithelial cells of the salivary glands, Ann N Y Acad Sci 1171 (2009) 407–414, https://doi.org/10.1111/j.1749-6632.2009.04688.x.

[19] K. Asadullah, W. Sterry, H.D. Volk, Interleukin-10 therapy—review of a new approach, Pharmacol Rev 55 (2003) 241–269, https://doi.org/10.1124/pr.55.2.4.

[20] A.J.G. Schottelius, M.W. Mayo, R.B. Sartor, A.S. Baldwin, Interleukin-10 signaling blocks inhibitor of κB kinase activity and nuclear factor κB DNA binding, Journal of Biological Chemistry 274 (1999) 31868–31874, https://doi.org/10.1074/jbc.274.45.31868.

[21] L. Mei, Y. Zheng, T. Ma, B. Xia, X. Gao, Y. Hao, Z. Luo, J. Huang, The novel antioxidant compound JSH-23 prevents osteolysis by scavenging ROS during both osteoclastogenesis and osteoblastogenesis, Front Pharmacol 12 (2021), https://doi.org/10.3389/fphar.2021.734774.

[22] S.S. Widodo, M. Dinevska, L.M. Furst, S.S. Stylli, T. Mantamadiotis, IL-10 in glioma, Br J Cancer 125 (2021) 1466–1476, https://doi.org/10.1038/s41416-021-01515-6.

[23] G.Q. Perrin, H.M. Johnson, P.S. Subramaniam, Mechanism of interleukin-10 inhibition of T-helper cell activation by superantigen at the level of the cell cycle, Blood 93 (1999) 208–216.

[24] P. Deshmukh, S. Unni, G. Krishnappa, B. Padmanabhan, The Keap1–Nrf2 pathway: promising therapeutic target to counteract ROS-mediated damage in cancers and neurodegenerative diseases, Biophys Rev 9 (2017) 41–56, https://doi.org/10.1007/s12551-016-0244-4.

[25] Y Salama, S Takahashi, Y Tsuda, Y Okada, K Hattori, B Heissig, YO2 Induces Melanoma Cell Apoptosis through p53-Mediated LRP1 Downregulation, Cancers (Basel) 15 (1) (2022 Dec 31) 288, https://doi.org/10.3390/cancers15010288.

[26] S.L. Harris, A.J. Levine, The p53 pathway: positive and negative feedback loops, Oncogene 24 (2005) 2899–2908, https://doi.org/10.1038/sj.onc.1208615.

[27] S. Kreuz, D. Siegmund, J.-J. Rumpf, D. Samel, M. Leverkus, O. Janssen, G. Hacker, O. Dittrich-Breiholz, M. Kracht, P. Scheurich, H. Wajant, NFκB activation by Fas is mediated through FADD, caspase-8, and RIP and is inhibited by FLIP, J Cell Biol 166 (2004) 369–380, https://doi.org/10.1083/jcb.200401036.

[28] S. Papoutsopoulou, L. Pollock, C. Walker, W. Tench, S.S. Samad, F. Bergey, L. Lenzi, R. Sheibani-Tezerji, P. Rosenstiel, M.T. Alam, V.A.P. Martins Dos Santos, W. Müller, B.J. Campbell, Impact of interleukin 10 deficiency on intestinal epithelium responses to inflammatory signals, Front Immunol 12 (2021), https://doi.org/10.3389/fimmu.2021.690817.

[29] M.S. Hayden, S. Ghosh, Regulation of NF-κB by TNF family cytokines, Semin Immunol 26 (2014) 253–266, https://doi.org/10.1016/j.smim.2014.05.004.

[30] H.-Y. An, H.-S. Shin, J.-S. Choi, H.J. Kim, J.-Y. Lim, Y.-M. Kim, Adipose mesenchymal stem cell secretome modulated in hypoxia for remodeling of radiation-induced salivary gland damage, PLoS One 10 (2015) e0141862, https://doi.org/10.1371/journal.pone.0141862.

[31] S.D. Tran, Y. Liu, D. Xia, O.M. Maria, S. Khalili, R.W.-J. Wang, V.-H. Quan, S. Hu, J. Seuntjens, Paracrine effects of bone marrow soup restore organ function, regeneration, and repair in salivary glands damaged by irradiation, PLoS One 8 (2013) e61632, https://doi.org/10.1371/journal.pone.0061632.

[32] D. Mansour Ghoneim, H. Raslan, O. Ramadan, I. Zeitoun, Expression of IL-10 and KI-67 in some benign and malignant salivary gland tumors "an immunohistochemical study,", Alexandria Dental Journal 0 (2022) https://doi.org/10.21608/adjalexu.2021.42308.1100, 0–0.

[33] H. Kang, M.-K. Seo, B. Park, S.O. Yoon, Y.W. Koh, D. Kim, S. Kim, Characterizing intrinsic molecular features of the immune subtypes of salivary mucoepidermoid carcinoma, Transl Oncol 24 (2022) 101496, https://doi.org/10.1016/j.tranon.2022.101496.

[34] L.S. Chard, N.R. Lemoine, Y. Wang, New role of Interleukin-10 in enhancing the antitumor efficacy of oncolytic vaccinia virus for treatment of pancreatic cancer, Oncoimmunology 4 (2015) e1038689, https://doi.org/10.1080/2162402X.2015.1038689.

[35] S. Yen Chong, Y.-C. Lin, J. Czarneski, M. Zhang, F. Coffman, F. Kashanchi, E. Raveche, Cell cycle effects of IL-10 on malignant B-1 cells, Genes Immun 2 (2001) 239–247, https://doi.org/10.1038/sj.gene.6363773.

[36] K.L. Legge, B. Min, J.J. Bell, J.C. Caprio, L. Li, R.K. Gregg, H. Zaghouani, Coupling of peripheral tolerance to endogenous interleukin 10 promotes effective modulation of myelin-activated T cells and ameliorates experimental allergic encephalomyelitis, J Exp Med 191 (2000) 2039–2052, https://doi.org/10.1084/jem.191.12.2039.

[37] M. Uhlén, L. Fagerberg, B.M. Hallström, C. Lindskog, P. Oksvold, A. Mardinoglu, Å. Sivertsson, C. Kampf, E. Sjöstedt, A. Asplund, I. Olsson, K. Edlund, E. Lundberg, S. Navani, C.A.-K. Szigyarto, J. Odeberg, D. Djureinovic, J.O. Takanen, S. Hober, T. Alm, P.-H. Edqvist, H. Berling, H. Tegel, J. Mulder, J. Rockberg, P. Nilsson, J.M. Schwenk, M. Hamsten, K. von Feilitzen, M. Forsberg, L. Persson, F. Johansson, M. Zwahlen, G. von Heijne, J. Nielsen, F. Pontén, Tissue-based map of the human proteome, Science (1979) (2015) 347, https://doi.org/10.1126/science.1260419.

[38] M. Redza-Dutordoir, D.A. Averill-Bates, Activation of apoptosis signalling pathways by reactive oxygen species, Biochimica et Biophysica Acta (BBA) - Molecular Cell Research 1863 (2016) 2977–2992, https://doi.org/10.1016/j.bbamcr.2016.09.012.

[39] Y.-H. Huang, M.-H. Chen, Q.-L. Guo, Z.-X. Chen, Q.-D. Chen, X.-Z. Wang, Interleukin-10 induces senescence of activated hepatic stellate cells via STAT3-p53 pathway to attenuate liver fibrosis, Cell Signal 66 (2020) 109445, https://doi.org/10.1016/j.cellsig.2019.109445.

[40] C. Rodriguez-Ramirez, Z. Zhang, K.A. Warner, A.E. Herzog, A. Mantesso, Z. Zhang, E. Yoon, S. Wang, M.S. Wicha, J.E. Nör, p53 inhibits bmi-1-driven self-renewal and defines salivary gland cancer stemness, Clinical Cancer Research 28 (2022) 4757–4770, https://doi.org/10.1158/1078-0432.CCR-22-1357.

[41] S.S. Khalid, Disrupted regulation of host cell cycle and its clinical significance in hepatitis C virus-related hepatocellular carcinoma, Gene Expr 000 (2023), https://doi.org/10.14218/GE.2022.00018, 000–000.

[42] S. Janssens, J. Tschopp, Signals from within: the DNA-damage-induced NF-κB response, Cell Death Differ 13 (2006) 773–784, https://doi.org/10.1038/sj.cdd.4401843.

[43] N.D. Perkins, Integrating cell-signalling pathways with NF-κB and IKK function, Nat Rev Mol Cell Biol 8 (2007) 49–62, https://doi.org/10.1038/nrm2083.

[44] S. Papoutsopoulou, L. Pollock, J.M. Williams, M.M.L.F. Abdul-Mahdi, R. Dobbash, C.A. Duckworth, B.J. Campbell, Interleukin-10 deficiency impacts on TNF-induced NFκB regulated responses in vivo, Biology (Basel) 11 (2022) 1377, https://doi.org/10.3390/biology11101377.

[45] F.Y. Yue, R. Dummer, R. Geertsen, G. Hofbauer, E. Laine, S. Manolio, G. Burg, Interleukin-10 is a growth factor for human melanoma cells and down-regulates HLA class-I, HLA class-II and ICAM-1 molecules, Int J Cancer 71 (1997) 630–637, https://doi.org/10.1002/(SICI)1097-0215(19970516)71:4<630::AID-IJC20>3.0.CO;2-E.

[46] L. Huynh, A. Kusnadi, S.H. Park, K. Murata, K.-H. Park-Min, L.B. Ivashkiv, Opposing regulation of the late phase TNF response by mTORC1-IL-10 signaling and hypoxia in human macrophages, Sci Rep 6 (2016) 31959, https://doi.org/10.1038/srep31959.

[47] C. Platzer, Ch Meisel, K. Vogt, M. Platzer, H.-D. Volk, Up-regulation of monocytic IL-10 by tumor necrosis factor-α and cAMP elevating drugs, Int Immunol 7 (1995) 517–523, https://doi.org/10.1093/intimm/7.4.517.

[48] V.P. Wagner, M.A.T. Martins, M.D. Martins, K.A. Warner, L.P. Webber, C.H. Squarize, J.E. Nör, R.M. Castilho, Overcoming adaptive resistance in mucoepidermoid carcinoma through inhibition of the IKK-β/IκBα/NFκB axis, Oncotarget 7 (2016) 73032–73044, https://doi.org/10.18632/oncotarget.12195.

[49] A. Naing, J.R. Infante, K.P. Papadopoulos, I.H. Chan, C. Shen, N.P. Ratti, B. Rojo, K.A. Autio, D.J. Wong, M.R. Patel, P.A. Ott, G.S. Falchook, S. Pant, A. Hung, K. L. Pekarek, V. Wu, M. Adamow, S. McCauley, J.B. Mumm, P. Wong, P. Van Vlasselaer, J. Leveque, N.M. Tannir, M. Oft, PEGylated IL-10 (pegilodecakin) induces systemic immune activation, CD8+ T cell invigoration and polyclonal T cell expansion in cancer patients, Cancer Cell 34 (2018) 775–791.e3, https://doi.org/10.1016/j.ccell.2018.10.007.

[50] Z. Strizova, M. Kuchar, L. Capkova, M. Komarc, J. Skrivan, J. Bartunkova, J. Plzak, D. Smrz, Fas-fas ligand interplay in the periphery of salivary gland carcinomas as a new checkpoint predictor for disease severity and immunotherapy response, Biomedicines 9 (2021) 402, https://doi.org/10.3390/biomedicines9040402.

[51] H.-M. Shin, M.-H. Kim, B.H. Kim, S.-H. Jung, Y.S. Kim, H.J. Park, J.T. Hong, K.R. Min, Y. Kim, Inhibitory action of novel aromatic diamine compound on lipopolysaccharide-induced nuclear translocation of NF-κB without affecting IκB degradation, FEBS Lett 571 (2004) 50–54, https://doi.org/10.1016/j.febslet.2004.06.056.

[52] H.A. Crissman, J.A. Steinkamp, RAPID, simultaneous measurement of DNA, protein, and cell volume in single cells from large mammalian cell populations, J Cell Biol 59 (1973) 766–771, https://doi.org/10.1083/jcb.59.3.766.

[53] H. Kim, X. Xue, Detection of total reactive oxygen species in adherent cells by 2′,7′-dichlorodihydrofluorescein diacetate staining, J Vis Exp (2020), https://doi.org/10.3791/60682.

[54] Z. Tang, C. Li, B. Kang, G. Gao, C. Li, Z. Zhang, GEPIA: a web server for cancer and normal gene expression profiling and interactive analyses, Nucleic Acids Res 45 (2017) W98–W102, https://doi.org/10.1093/nar/gkx247.